Geopolymer beads and 3d printed lattices containing activated carbon and hydrotalcite for anionic dye removal

Oliveira Karine G., Botti Renata, Kavun Vitalii, Gafiullina Anastasiia, Franchin Giorgia, Repo Eveliina, Colombo Paolo

DOI: 10.1016/j.cattod.2021.12.002

GEOPOLYMER BEADS AND 3D PRINTED LATTICES CONTAINING ACTIVATED CARBON AND HYDROTALCITE FOR ANIONIC DYE REMOVAL

Karine G. Oliveira[a]; Renata Botti[b]; Vitalii Kavun[c]; Anastasiia Gafiullina[c]; Giorgia Franchin[b*]; Eveliina Repo[c]; Paolo Colombo[b,d]

[a]Fibre and Particle Engineering Research Unit, University of Oulu, Pentti Kaiteran katu 1, 90570, Oulu, Finland.
[b]Department of Industrial Engineering, University of Padova, via Francesco Marzolo 9, 35131, Padova, PD, Italy.
[c]Department of Separation Science, LUT University, Yliopistonkatu 34, 53850, Lappeenranta, Finland.
[d]Department of Materials Science and engineering, The Pennsylvania State University, University Park, PA 16802.

*Corresponding author: giorgia.franchin@unipd.it

Abstract

The use of geopolymers as adsorbent materials has been increasingly investigated in the last few years, thanks to their highly intrinsic mesoporosity and ion exchange capability. As they consolidate following a condensation reaction from a liquid slurry, they can easily be used as a binder for widely known adsorbents, such as zeolites or activated carbons. Such combination is very promising for applications in the field of water treatment. Geopolymer slurries consolidate at room temperature and can be easily shaped using different fabrication techniques.

In this work, the performance of geopolymer composites with the addition of activated

bentonite as a rheological agent to enhance the pseudoplasticity of the ink. The lattices were printed with a nozzle with a diameter of 840 μm and consisted of a 0º - 90º stacking of layers of filaments with 0.8 mm spacing, which resulted in a design porosity of 50 vol%; the geopolymerization was completed at 75 ºC for 2 days and 100% relative humidity.

Physical and chemical characterizations were performed on both beads and lattices (porosity, morphology and crystallinity, compressive strength); the removal efficiency of Orange II dye was evaluated focusing on the adsorption capacity and kinetics.

Keywords: Additive manufacturing; geopolymers; water treatment; adsorption; dye removal.

1. Introduction

Since the industrial revolution in the 18th century, the production of industrial wastes has increased exponentially. The growth of industries such as mining and metallurgical, electronic, textile, agricultural, pharmaceutical, cosmetics and many others are the main cause of soil and water contamination. Metal ions, anionic metal complexes and other species [1], herbicides, antibiotics and dyes [2] are examples of contaminants that are currently found in drinking water, putting at risk human health and the environment. According to the United Nations, in the developing countries, around 80% of all industrial and municipal wastewaters are released into the environment without any kind of pretreatment. Additionally, water pollution is also increased by urban stormwater runoff, agricultural runoff, and polluted rainwater that can reach drinking water sources. The threats of contamination of the available drinking water are numerous; however, industrial waste derived pollution is one of the most concerning and growing dangers in our time.

One of the examples of such threatening pollutants are synthetic dyes that are in extensive use not only in the textile industry, but also the leather, rubber, plastic, cosmetics, paper and printing ones as well [3]. Dyes constitute a danger due to their interactions with sunlight in

chemicals or energy, generation of process wastes or potentially harmful by-products. Adsorption represents an overall non-harmful treatment technique possessing high efficiency due to the ability to tune an adsorbent towards a particular pollutant and to its high efficiency even for highly diluted solutions. On the other hand, it is essential to evaluate adsorbent-adsorbate interactions under variable process conditions, such as solution pH, temperature and composition (presence of natural organic matter (NOM), ionic nature). Although water contamination is commonly associated with industrial wastewaters, it is also frequently reported in other water sources, such as domestic wastewater effluents, groundwater, rivers and lakes [7–12]. All the mentioned water sources possess different water quality characteristics, which makes the adsorbent-adsorbate interactions in real water matrices very complex and affects the adsorption performance.

A variety of materials are widely used as adsorbents for the removal of industrial contaminants, such as clays, activated carbon, biochars, resins, zeolites, etc. Recent trends focus on investigating the adsorption properties of bio-based materials [13,14], synthesized highly porous framework materials [15,16], and geopolymers [17,18].

Geopolymers (GPs) were first introduced by J. Davidovits in late 1970's to describe an inorganic material constituted by an amorphous aluminosilicate three-dimensional network with structural mesoporosity (i.e. pore diameters in the 2-50 nm range)[19]. Their network consolidates at ambient conditions and does not require further sintering at elevated temperatures; moreover, they can be synthetized from waste materials such as fly ashes, biomass ashes and foundry slags. For these reasons, they represent a low cost and environmentally friendly alternative for water treatment compared with conventional materials such as synthetic zeolites, ceramics and polymers. Sorption capabilities of geopolymers are related both to their mesoporosity and their cation exchange ability. In fact, an exchange of silicon for aluminum in the network results in negatively charged sites compensated by alkali cations which become available for transport within the GP structure.

Activated carbon is the state-of-the art adsorbent choice for anionic pollutants, due to its excellent performance that comes from its highly developed micro and mesoporous structure, which determines a large specific surface area as well as the presence of different active sites (i.e., functional groups such as carboxyl, carbonyl, phenol, etc.) anchored to the surfaces of the graphite-like layers, which can be tailored for specific adsorption.

Hydrotalcite is a double-layered mixed mineral of the clay family, with anionic nature. Solid inorganic hydrotalcites are constituted of layers of $Mg(OH)_2$, in an octahedral structure similar to that of brucite. The main feature of hydrotalcites is their great anion exchange capacity. For this reason, they are often used as anionic pollutant adsorbents in advanced wastewater treatment.

Activated carbon and hydrotalcite are often supplied as powders, and their cost is generally higher than that of a geopolymer. Another major advantage of geopolymers is the ease of shaping, which can result in optimized geometries and morphologies for water treatment [31].

Beads can be produced by dropping a geopolymer slurry into a bath that ensures a rapid consolidation of the droplet spherical shape; in the case of a liquid nitrogen bath, consolidation happens via levitation on a supporting vapor layer following the “inverse” Leidenfrost effect [32]. Moreover, the water present in the geopolymer slurry results in segregation and directional freezing of ice from the external surface of the bead towards the warmer center. Upon ice sublimation, an oriented (radial) porosity is developed in the bead [26]. In industrial applications, the use of porous beads could facilitate separation steps in comparison with powders and increase efficiency compared to monoliths [33].

Another method to produce geopolymer components with high open porosity is additive manufacturing (AM) [34]. With AM, it is possible to precisely control the pore size, pore-size distribution, pore shape, and pore interconnectivity; non-stochastic porosity generally results in higher strength and optimized permeability and tortuosity with respect to foams. Geopolymer slurries are ideal candidates for extrusion-based AM processes such as Direct Ink Writing

to the geopolymer intrinsic mesoporosity. The influence of the material choice as well as the geometry and morphology on the removal of an organic, anionic dye (Orange II) from water was evaluated.

2. Materials and methods

2.1 Fabrication Method – Beads by Freeze-drying

The geopolymer slurry employed as matrix for the composite beads had the following composition (molar ratios): Na_2O/SiO_2 = 0.263; SiO_2/Al_2O_3 = 3.8; Na_2O/Al_2O_3 = 1 and H_2O/Na_2O = 25.

First, an alkaline solution was prepared by mixing pellets of sodium hydroxide (NaOH, Sigma-Aldrich, Steinheim, Germany) with a sodium silicate solution (SS 2942, Ingessil S.r.l., Montorio, Italy) and distilled water. The solution was prepared and stored at 4 °C at least 24 h prior to its use. Then, the slurries were prepared by adding metakaolin (Argical 1200S, Imerys S.A., Paris, France), to the alkaline solution and mixing for 10 min at 2200 rpm. Afterwards, either activated carbon (C242, CAM Italia Spa) or hydrotalcite (Sigma Aldrich GmbH) were added and mixed for another 10 minutes, in order to obtain samples B_GP_C242 (21.5 wt.% C242, dry basis) and samples B_GP_H (22.8 wt.% hydrotalcite, dry basis) respectively.

The slurries were dripped with a pipette into a liquid nitrogen bath, where they were immediately shaped into beads. They were then transferred into a freeze dryer (Labconco, FreeZone 2.5 Liter Benchtop Freeze Dry System, Kansas City, USA) at -52 °C and 0.2 mbar of pressure for 48 hours. After that, the beads were moved in an oven at 75 ºC and 100% relative humidity for another 48 hours to allow for curing.

2.2. Fabrication Method – Lattices by Additive Manufacturing

The geopolymer matrix in the lattices produced by additive manufacturing (direct ink writing, DIW) had the same composition of the previous one (molar ratios): Na_2O/SiO_2 = 0.263;

water bath (to slow down the geopolymer reaction), and mixed for 10 min. The different percentage of filler between the different materials and fabrication processes derives from the highest admissible content which can be added in order to obtain a homogeneous mixture with optimal viscosity for dripping or extruding.

The obtained slurries were loaded into a syringe and mounted on a DIW 3D printer (Delta Wasp 2040 Turbo, Wasproject, Massa Lombarda, IT) equipped with a pressure vessel and a screw extrusion system. The machine was configured with print speed in a range of 7 to 10 mm/s and extrusion flow as needed. Lattice structures were printed at room temperature and in ambient air. The ink was extruded through the tip of a conical nozzle with a diameter of 840 μm (Nordson Italia S.p.a., Segrate, IT). The printed lattices were constituted of layers of parallel geopolymer filaments with a 0.8 mm spanning distance. The design porosity was obtained considering the sample as a solid cube, the volume occupied by the material was the dimension of the filament (0.8mm), and the void volume was the space between the filaments (0.8mm), therefore the design porosity was 50%; each layer was stacked at a 90º angle with respect to the previous one. The lattices designed dimensions were 20 mm (side) and 9.6 mm (height). The printing process is described in detail elsewhere [35]. After printing, the samples were placed in a muffle furnace at 75 °C for 2 days in a closed environment to complete the geopolymerization reaction.

The same slurries produced for DIW were poured into a closed mold, cured at 75 °C for 2 days and then ground in order to produce a powder which was used in the adsorption test to evaluate the performance of the materials themselves (P_GP_C242 and P_GP_H).

Fig. 1 shows the general procedure followed to fabricate beads and lattices with activated carbon and hydrotalcite.

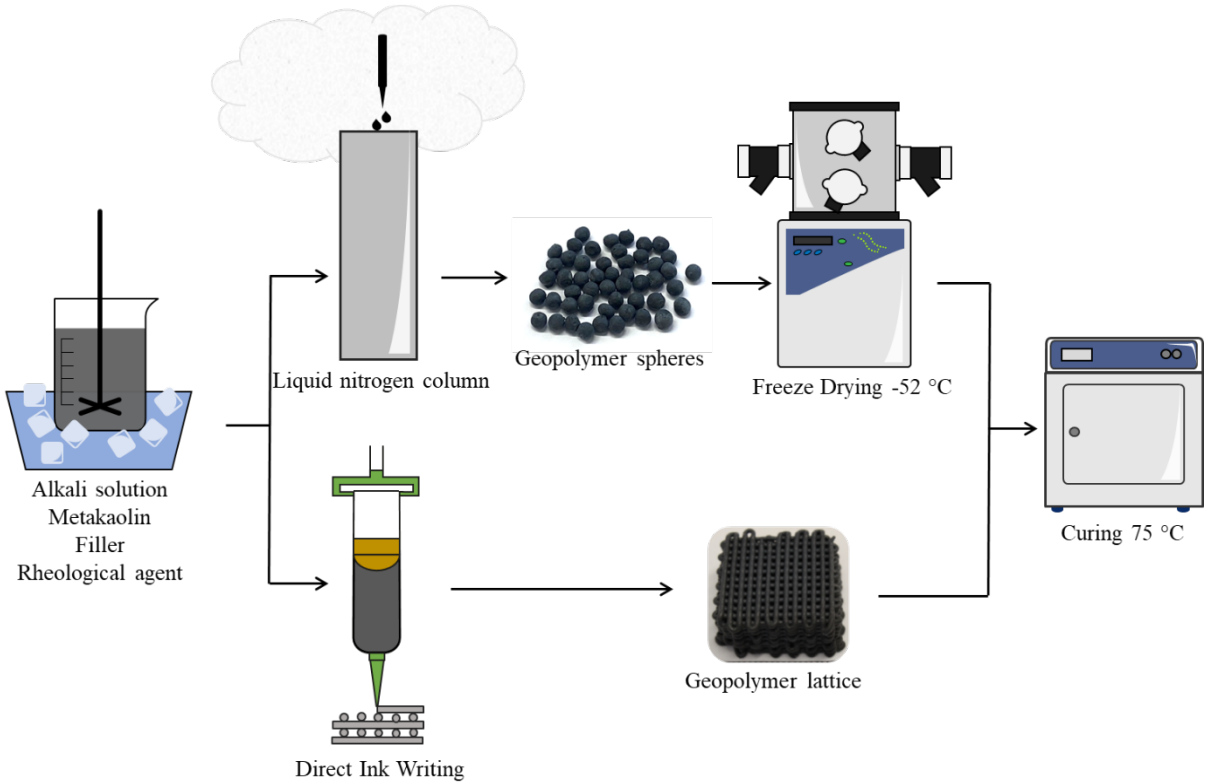

Figure 1. Manufacturing process for geopolymer beads and lattices.

2.3. Characterization

The amorphous structure and/or the crystalline phase assemblage of the geopolymer composites, were identified on ground and sieved beads by an X-ray diffractometer (D8 Advance, Bruker Corporation, Karlsruhe, Germany) with Cu-Kα radiation, operated at 40 kV and 40 mA with 0.05° step width, a scanning range of 10 - 70° and a scanning speed of 1 s/step.

Physical and chemical characterizations were performed on both beads and lattices. The apparent (ρ_a) and true (ρ_t) density of the beads was measured using a helium pycnometer (Micrometrics AccuPyc 1330, Norcross, GA, USA) on entire beads or lattice parts and on crushed powders, respectively. The bulk or geometric density (ρ_g) was obtained by dividing the

Specific surface area (SSA) was determined by multi-point Brunauer, Emmett, Teller (BET) method with Quantachrome Autosorb iQ (Quantachrome Instruments, Boynton Beach, Florida), with a degassing temperature of 110 °C for approximately 16 h under reduced pressure and analysis by N_2 adsorption at liquid nitrogen temperature.

The morphology of all samples was analyzed through optical microscopy (STEMI 2000-C, Carl Zeiss AG, Oberkochen, DE) and scanning electron microscopy (ESEM, Quanta 200, FEI, Hillsboro, OR), with a magnification varying from of 25x to 5000x. Chemical analysis was also carried out by energy-dispersive X-ray spectroscopy (EDX).

To evaluate the degree of geopolimerization of the samples, FTIR measurements were carried out on ATR-FTIR spectrometer (ATR Pro ONE attachment, FTIR6200, JASCO, Japan); the infrared range of the analysis was 4000 to 600 cm^{-1} with a spectral resolution of 4 cm^{-1}, recording 64 scans.

2.5. Adsorption Tests

Synthetic solutions with different dye initial concentrations for pH, isotherm and kinetic experiments were prepared by dissolving Orange II sodium salt (C16H11N2NaO4S, dye content > 85%, Sigma-Aldrich) in ultra-pure deionized water (0.5 - 1 µS/cm at 25 °C) collected from CENTRA-R 60/120 system (Elga treatment system, Veolia Water, Bucks, UK). Diluted HCl (pure grade, 37%, PCC Rokita SA) and NaOH (water solution, 50 wt.%, Sigma-Aldrich) were used to adjust pH of the solutions. Adsorbents produced as described above were dried in a vacuum oven at the temperature of 105 °C for 24 hours and then kept in desiccator prior to the analyses. Powder samples were additionally milled in an agate mortar to assure that there were no changes in the geopolymers' surface area due to the potential particle aggregation.

Adsorption experiments were run in a batch mode. The main studied parameter was the performance of a particular type of adsorbent – GP_H or GP_C242, available in three configurations (powder (P), beads (B), lattices (3D)) – under variable experimental conditions. Namely, the influence of the pH and concentration of the initial solution and of the contact time

The effect of contact time was investigated for 100 mg/L and 150 mg/L dye solutions mixed with GP_H and GP_C242 materials, respectively. The samples of the treated solutions were collected at 5, 15, 30, 60, 120, 240, 480, and 1440 min.

Prior to analytical determination of the residual Orange II content, the collected samples were filtered through 0.45 mm regenerated cellulose syringe filters, and the final solution pH was measured. The solution pH was measured by a digital Metrohm 744 pH Meter (Switzerland) at 25 °C. UV/Vis spectrophotometer (Jasco V-670 spectrophotometer, Japan) was utilized to measure the concentration of Orange II dye solutions before and after adsorption at λ = 510, 470 and 315 nm.

Adsorption capacity of the adsorbent material at time t (q_t, mg g^{-1}) was calculated according to Eq. (3):

$$q_t = \frac{(C_0 - C_t) \times V}{m} \tag{3}$$

where C_t is the concentration of the studied substance (Orange II) in the solution at time t (mg·L^{-1}), V is the volume of the solution (L), and m is the mass of the geopolymer used in the adsorption test (g).

The effect of usage on the geopolymer components was evaluated by repeating compressive strength tests, total porosity calculation and SSA determination on samples subject to the equilibrium adsorption capacity experiment with initial concentration of 25 mg/L.

3. Results and discussion

3.1. Geopolymer composites synthesis

Fig. 2 shows the XRD spectra of ground B_GP_C242 and B_GP_H samples (for the spectra of metakaolin, C242 and hydrotalcite raw materials see the Supplementary Information, Fig. S1a). The typical spectrum of metakaolin based geopolymers can be identified in both samples, with an amorphous band centered at about 27° and the characteristic peaks of metakaolin impurities (quartz, anatase and muscovite). The amorphous nature of the activated carbon, with a band centered at similar angles, makes it difficult to assess its presence; on the

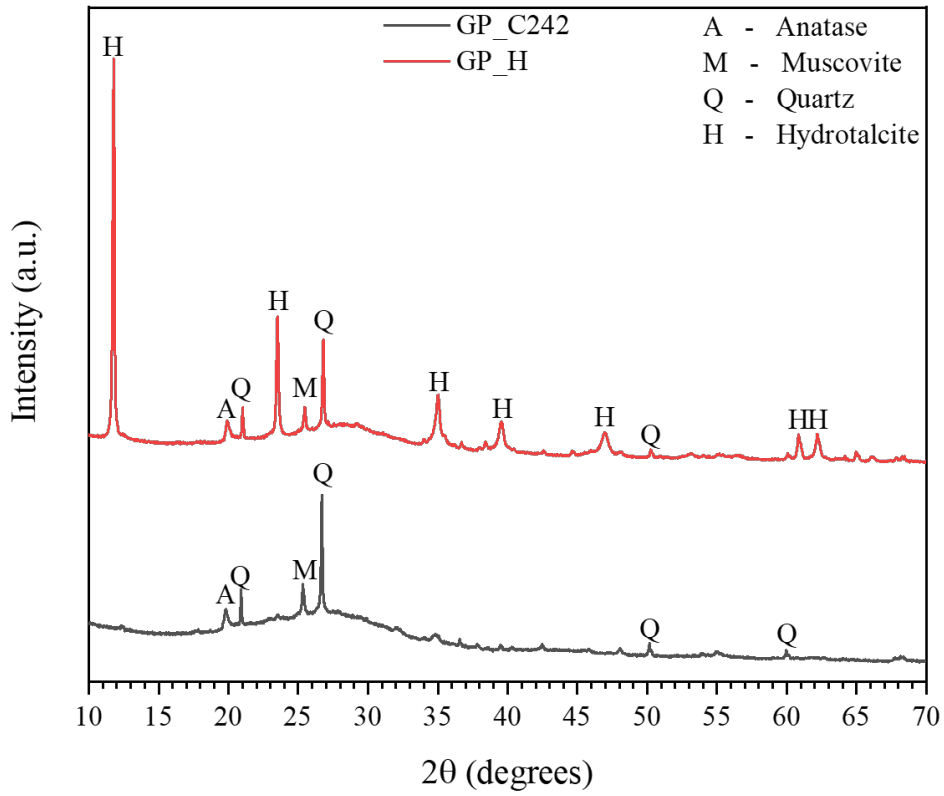

Figure 2. XRD patterns for B_GP_C242 and B_GP_H.

3.2. Beads by Freeze-drying

SEM images of a B_GP_C242 bead are shown in Fig. 3; the bead appears spherical with a smooth surface (Fig. 3a). The measured diameter of both B_GP_C242 and B_GP_H beads was 4.1 ± 0.1 mm; the low standard deviation is a confirmation of the repeatability of the freeze-drying technique. The average weight of a B_GP_C242 bead was 44 ± 3 mg. The surface of the bead appears only slightly porous (Fig. 3b), whereas the internal core appears highly porous (Fig. 3c); the pores are left by the water that was extracted during the freeze-drying process. There is a homogeneous distribution of the activated carbon within the geopolymer matrix; in Fig. 3d, the red circle highlights a particle of activated carbon with a distinctive cellular

typical path for the crystallization of ice and subsequent extraction of the water during freeze-drying process.

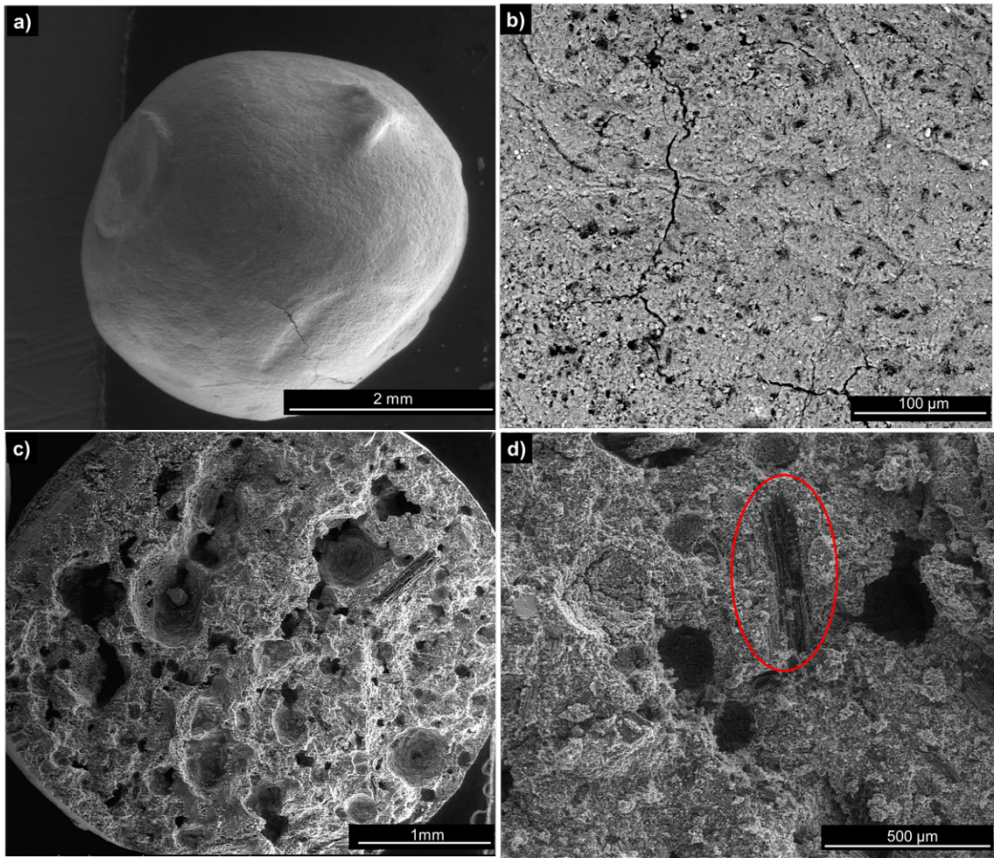

Figure 3. SEM images of B_GP_C242: (a-b) external surface and (c-d) internal core.

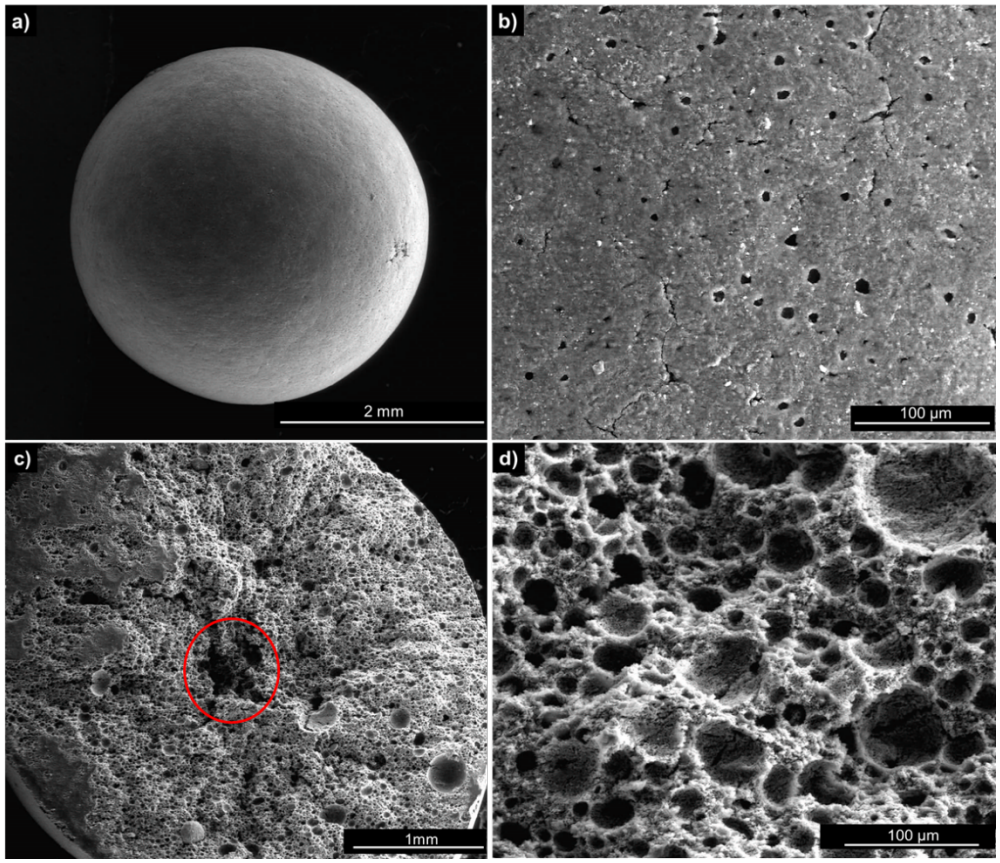

Figure 4. SEM images of B_GP_H: (a-b) external surface and (c-d) internal core.

Table 1 reports the results of the compressive strength, total and open porosity, and specific surface area (SSA) of B_GP_C242 and B_GP_H beads. It appears that for both samples the porosity is almost entirely open and interconnected. Beads with activated carbon confirmed lower porosity values compared to those with hydrotalcite; this could be related to water separation in the slurry and might be solved by adding a surfactant to it. As a result, their compressive strength was higher. Even though the macro-porosity was lower, the SSA for the B_GP_C242 beads was much higher, certainly due to the high SSA of the activated carbon.

presence of water, yet water was removed from the beads during the freeze-drying process; therefore, additional water must be provided in order for the beads to react properly. The most characteristic region for both metakaolin and geopolymers is at about 1000 cm^{-1}, attributed to asymmetric stretching vibrations of Si–O–Si and Al–O–Si. For the metakaolin, this peak is centered at about 1050 cm^{-1}, while for a cured geopolymer it generally shifts to lower wavenumber (about 990 cm^{-1}) due to the formation of the amorphous aluminosilicate gel [38].

When the beads were cured at 100% RU, the peak was centered at 987 cm^{-1}; when they were cured without humidity, the peak remained closer to that of metakaolin (1015 cm^{-1}); this confirms that curing must be performed at 100% RU to produce stable, fully reacted components.

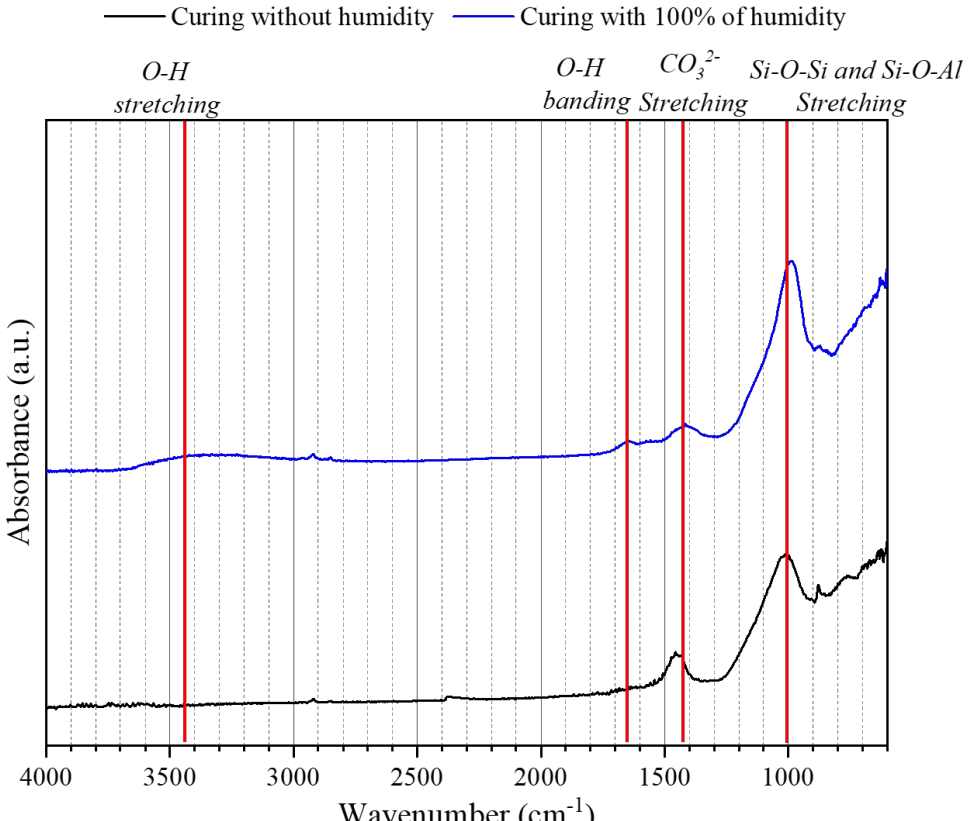

process. The measured dimensions of 3D_GP_C242 and 3D_GP_H lattices were 19.8 ± 0.4 mm (side) and 9.3 ± 0.5 mm (height), showing good accordance with the design.

The rheological behavior of geopolymer composite inks with similar composition and filler fraction was described elsewhere [38], and it was proven to be suited for DIW of similar lattice structures. Fig. 6b confirms that the filament is able to maintain its shape without sagging even in the case of suspended bridges, keeping the macroporosity open also in the Z direction. At higher magnification (Fig. 6c), the cross section of a strut shows additional macro-voids, due to mixing, as well as the presence of activated carbon (highlighted in the red circle).

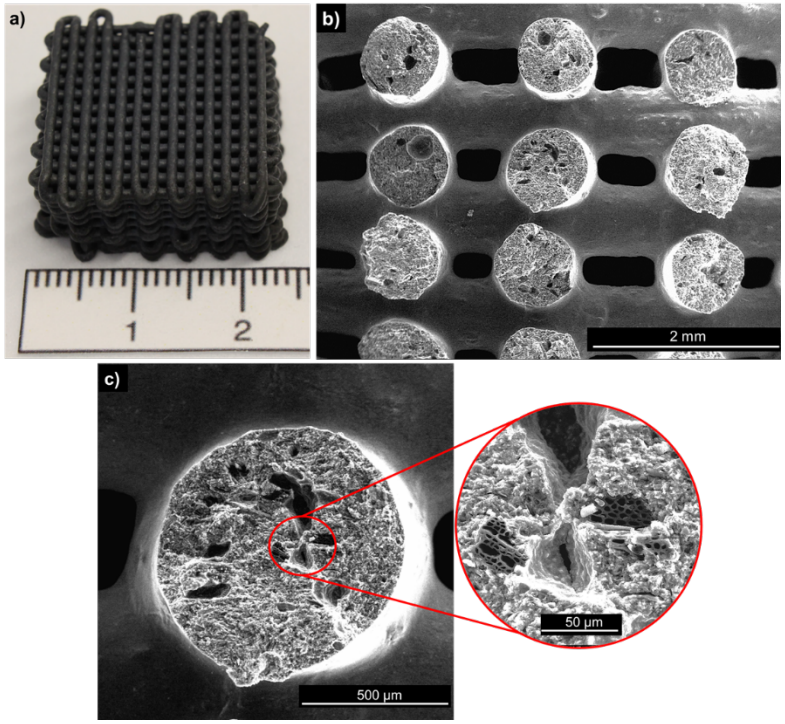

Figure 6. (a) Image of 3D_GP_C242 lattice; **(b-c)** cross section of 3D_GP_C242.

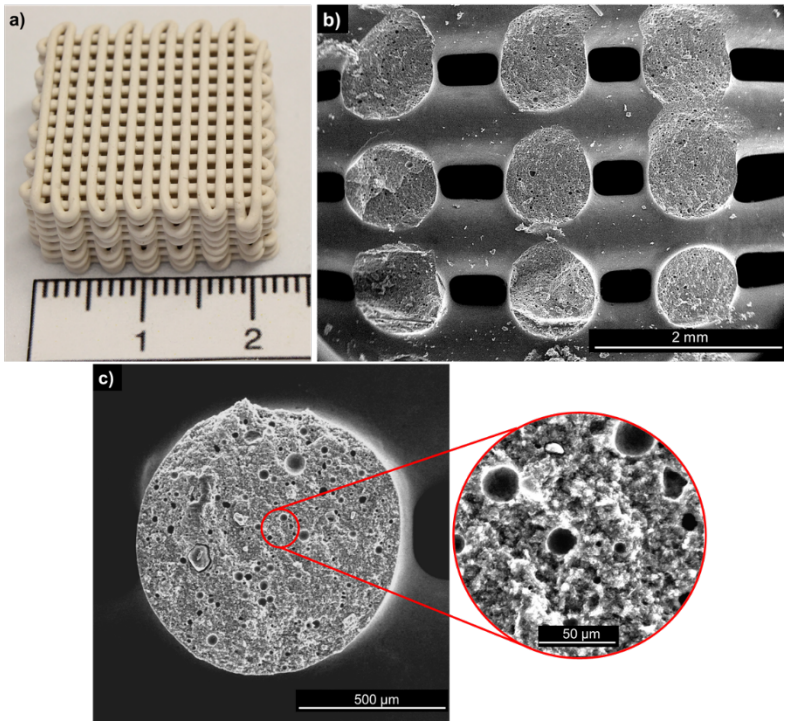

Figure 7. (a) Image of 3D_GP_H lattice; **(b-c)** cross section of 3D_GP_H.

Table 2 reports the results of the compressive strength, total and open porosity, and SSA of 3D_GP_C242 and 3D_GP_H lattices. As for the beads, the porosity of the printed lattices is almost entirely open. The macroporosity was set at 50% by design, therefore it appears that the struts possess some intrinsic porosity related to the entrapment of air but also to the evaporation of water during consolidation; in fact, 3D_GP_C242 lattices have a higher water ratio than 3D_GP_H and a slightly higher porosity. A high amount of open, interconnected porosity should provide high contact area between the lattice and the water to be treated, hence a great reach on the active fillers and a high removal efficiency. In addition, the chosen geometry is known to have higher permeability compared to monolithic adsorbents and packed beds [37].

slurries with higher water ratios and porous fillers. Their compressive strength is in agreement with the previous results if the higher porosity value is considered; it is higher than that of the beads and in any case sufficient for the intended application.

Similar to the beads, lattices with activated carbon show a much higher SSA compared to those with hydrotalcite. The SSA values of the lattices are higher than those of the corresponding beads; the denser skin produced by freeze-drying appears to partially close access to the microporous fillers. 3D_GP_C242 lattices are expected to be the best candidates for an adsorption-driven dye removal; 3D_GP_H might still provide anion exchange capabilities.

3.4. Adsorption Tests

3.4.1. Effect of solution pH on adsorption of Orange II

Assessment of adsorption efficiency of the materials was started from optimizing the pH of the solution. This parameter has a prominent influence on adsorption processes by protonation and deprotonation of dissolved substances and solid materials, changing their surface charge and accessibility of binding sites of the solid phase. Therefore, the sorption studies of the anionic dye and performance of ground geopolymers P_GP_C242 and P_GP_H were conducted in wide pH range, from 1 to 9.

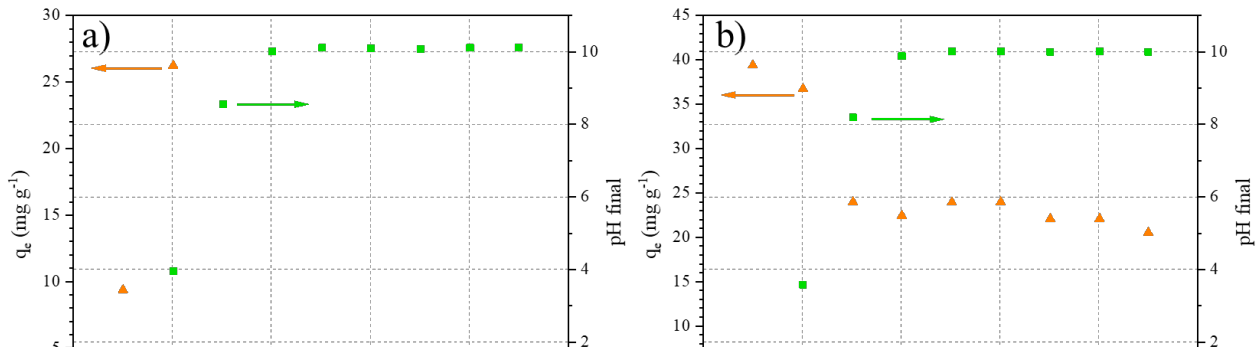

The experimental data presented in Fig. 8 clearly demonstrate the strong pH dependent behavior for both materials. Despite the highest adsorption capacity of 39.4 mg g^{-1} for P_GP_C242 at pH 1 and 26.2 mg g^{-1} for P_GP_H at pH 2, the removal efficiency decreased by 44% and 94%, respectively, after pH 3. At the same time, both adsorbents showed similar trend of increased alkalinity of solution within the pH range 3 – 9 after adsorption experiments. This similar behavior could be attributed to the presence of the same metakaolin geopolymer matrix, and not to the filler component.

It is well-known that alkaline activated materials are prone to an ion-exchange, releasing Na^+ ions into solution from both interlayer and surface sites [39] and exchanging with protons from aqueous solutions that facilitate the increase of pH. Therefore, the apparent rise of solution pH after adsorption experiments at pH > 3 (see final pH in Fig. 8) can be ascribed to the formation of excess OH^- ions. This, in turn, leads to the lower adsorption of anionic dye due to deprotonation and formation of negatively charged surface sites on the materials, and, thus, electrostatic repulsion between the adsorbent and the adsorbate. However, at acidic conditions only a moderate increase of the final pH is observed, and it does not significantly affect the final adsorption capacity of the materials. This fact can be ascribed to the high proton concentration that is sufficient for both ion-exchange and protonation of the adsorbent surface.

Although the assessment of material performance is usually investigated under the most favorable pH conditions, pH 2 was set for further adsorption experiments for both materials so their performance under uniform conditions can be compared. Moreover, shifting pH to highly acidic range requires concentrated chemicals in sufficient amount, which increases exponentially when pH tends to 0. It does not contribute neither to the environmental part of the process nor the economical one.

The adsorption efficiency at lower pH can be explained via electrostatic interactions between the adsorbent and the adsorbate. The aluminosilicate network of geopolymers carries negative surface charge, balanced by Na^+ ions. The weak increase of pH after adsorption

The results are consistent with the literature on adsorption of different anionic species onto geopolymers and carbon-based materials, where the most favorable conditions were found at very low pH values [28,30,43–45].

3.4.2. Adsorption isotherms

To estimate the maximum adsorption capacity of powder materials and compare the recovery efficiency with adsorbents in the shape of beads and lattices, the adsorption isotherms were derived by plotting the equilibrium adsorption capacities of the solid phase (q_e, mg g^{-1}) against the equilibrium concentration of Orange II present in the supernatant (C_e, mg L^{-1}) after an adsorption experiment, as reported in Fig. 9.

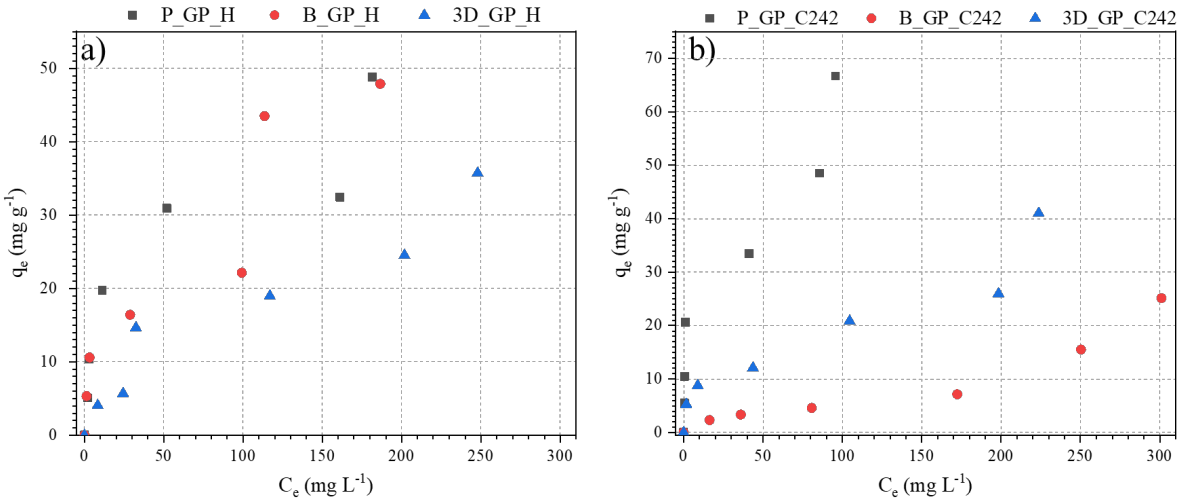

Figure 9. Adsorption isotherms for geopolymer adsorbents filled with hydrotalcite **(a)** and activated carbon **(b)**; pH 2, 24 h.

Maximum achieved experimental adsorption capacities of 48.82 and 66.65 mg g^{-1} were observed for P_GP_H and P_GP_C242, respectively, in the treatment of initial 400 mg L^{-1}

g $^{-1}$), that can be ascribed to the open porous structure of the B_GP_H (see Section 3.2) facilitating the external/internal diffusion of anionic dye molecules to the adsorption sites.

Different sorption models with two or more unknown parameters for mono- and multilayer adsorption were applied to fit the equilibrium data. However, only some of the models showed reasonable fitting parameters, which are summarized in the supplementary information (Figs. S2, S3, Table S1). The slope of the isotherms along with $R_L > 0$ suggest energetically favorable adsorption for all the materials. The shape of the isotherms is similar to Type II adsorption isotherms, corresponding to the heteroporous solids, and, thus, cannot be reasonably fitted by adsorption models limited to a monolayer adsorption ($R^2 < 0.93$). Besides, at high C_e values all the materials demonstrated a noticeable increase in the equilibrium adsorption capacity. In comparison to other multilayer adsorption models, the extension of the Brunauer–Emmett–Teller (BET) isotherm model for solid-liquid interface showed appropriate ($R^2 > 0.94$) fitting to the experimental data. The model suggests the homogeneous distribution of active sites and the uniform adsorption energy for all sites in the same layer. The adsorption energy of the first layer is different from the second and other layers, while the adsorbent-adsorbate interactions do not have a direct influence on the formation of subsequent adsorbate-adsorbate layers [46]. The fitting of experimental data of B_GP_C242 to the BET model revealed that the monolayer adsorption capacity (q_m = 4.85 mg g^{-1}) is almost 5 times lower compared to B_GP_H (q_m = 21.51 mg g^{-1}). The fact of well-fitted data by multilayer adsorption model may indicate the presence of additional π – π adsorbate-adsorbate interactions along with electrostatic attraction to the surface of the adsorbent [47].

3.4.3. Adsorption kinetics

Kinetic experiments with geopolymer based materials were performed to determine the rate-controlling stage during the adsorption process. The contact time was varied from 5 min to 24 h at 100 and 150 ppm solutions for GP_H and GP_C242 adsorbents. The equilibrium time

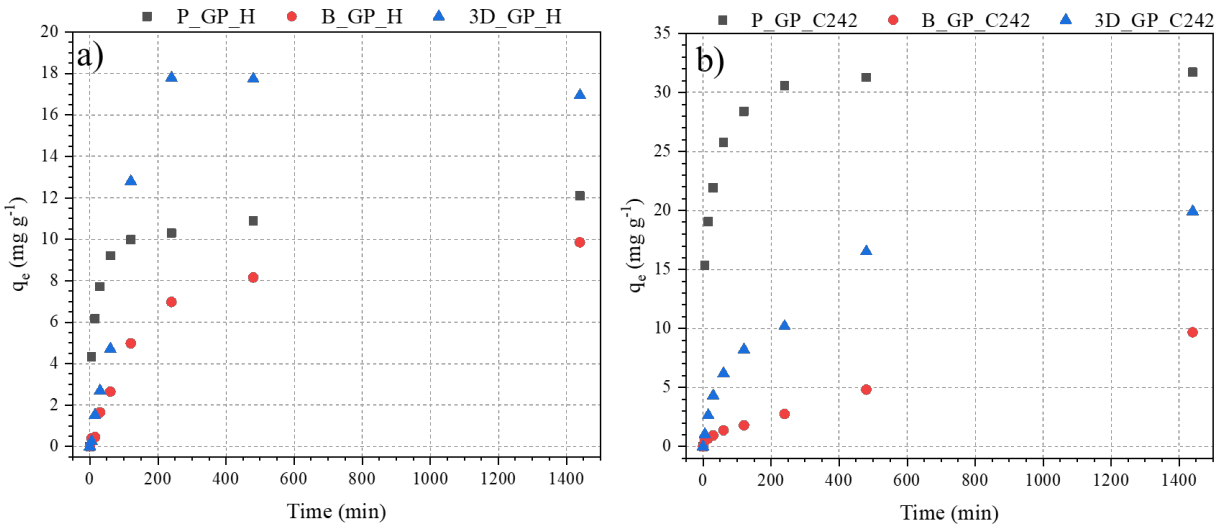

Figure 10. Effect of contact time on adsorption of Orange II by geopolymers filled with hydrotalcite **(a)** and activated carbon **(b)** for 100 and 150 ppm solutions, respectively (data collected at pH 2).

Fitting of the experimental data for all the materials was performed using several kinetic models. The results of the modelling along with calculated kinetic constants and R^2 values are summarized in the supplementary information (Figs. S4, S5, Table S2). The kinetic data were well fitted ($R^2 > 0.97$) to the pseudo-second-order model for all the materials except 3D_GP_H, which is better described by the pseudo-first-order kinetic model. At the same time other applied models did not show a reasonable correlation with experimental data, generally showing $R^2 < 0.95$, and, therefore, are not further discussed. The fitting by PSO model indicates that the materials are abundant with surface active sites [48] and kinetics of adsorption of Orange II is dependent on the rate of the reaction between adsorbate and adsorbent, which is mostly driven by electrostatic attractions.

The rate and the uptake of the pollutant by activated carbon filled GPs increases in the

results of adsorption isotherms studies (see Section 3.4.2), where B_GP_C242 demonstrated the lowest experimental q_e and calculated monolayer adsorption capacities. Higher adsorption capacities were measured for 3D_GP_C242, which might be due to the higher surface area to volume ratio, thus more external surface area was available for adsorption. Additionally, more porous external surface (due to absence of the freeze-drying step) resulted in better accessibility of internal porous space and faster adsorption kinetics. Finally, the highest capacities exhibited by the P_GP_C242 samples may be attributed to the largest available SSA, which was due to the very small size of the particles and to the internal porosity open for contact with adsorbate.

Similar reasons may be behind higher adsorption capacities of 3D_GP_H over the B_GP_H (calculated initial PSO rate: 0.19 > 0.06 mg g^{-1} min^{-1}). Unlike activated carbon [49], powdered hydrotalcite does not possess developed internal porosity, which was confirmed by the SEM analyses in the following works [50,51]. It might happen that SSA of P_GP_H is comparable with those of B_GP_H due to the fact that the internal porosity is either nonexistent or inaccessible, while the kinetic rate is the highest due to easily accessible active sites on the powder surface (initial PSO rate: 0.37 mg g^{-1} min^{-1}). At the same time, differences in the synthesis of 3D_GP_H led to formation of partially available internal porosity that may reflect on the performance of the lattices at moderate concentrations.

3.4.4. Stability of the sorbents upon usage

Table 3 reports the results of the compressive strength, total porosity, and SSA of the beads and of the 3D lattices after usage. The mechanical properties of the geopolymer samples decreased after the exposure to high acidic environment and the adsorption of the dye. Such decrease is more pronounced in samples with higher total porosity, up to -72% for 3D_GP_C242, as a result to higher accessibility and penetration of the dye solution into the structure. The total porosity also increased for all samples, with a higher variation for those containing hydrotalcite (~21% *vs* ~13% for those containing C242). A major difference could

Table 3. Physical properties after usage of beads B_GP_C242 and B_GP_H and lattices 3D_GP_C242 and 3D_GP_H.

Samples	Compressive Strength [MPa]	Variation in Compressive Strength	Total Porosity [%]	Variation in Total Porosity	SSA [$m^2 g^{-1}$]	Variation in SSA
B_GP_C242_used	1.1 ± 0.4	-48%	53.8 ± 0.1	+13%	349.2	+215%
B_GP_H_used	1.0 ± 0.3	-23%	66.36 ± 0.03	+23%	3.5	-10%
3D_GP_C242_used	2.1 ± 0.5	-60%	75.5 ± 0.02	+12%	331.9	+79%
3D_GP_H_used	1.5 ± 0.4	-72%	74.56 ± 0.02	+18%	19.4	-24%

From the XRD spectra of the two materials before and after the adsorption tests (see Fig. S1b-c), a slight decrease in intensity of the amorphous band could be detected; this is attributed to the electrophilic attack by acid protons on the Si-O-Al bonds of the geopolymer matrix, resulting in the ejection of aluminum from the framework [52]. The degradation of the matrix can be held responsible for both the decrease in mechanical strength and the increase in porosity of the components. The increase in intensity of the amorphous band of C242 at lower angles can be associated with a higher exposition of the filler, resulting in the increased SSA. The low SSA of hydrotalcite with intercalated water reflects in the low values of the GP_H composites even after the degradation of the matrix [53].

No significant difference could be detected for prolonged permanence in the acidic dye solution, a sign that the components could be reused for additional cycles.

4. Conclusion

Geopolymer composite components with the addition of activated carbon and hydrotalcite were fabricated in different shapes (beads and 3D lattices) and tested for the removal of the

the surface of the spheres, however, appears less porous and might hinder the accessibility to the inner core.

Lattices were fabricated by DIW of geopolymer composite slurries. The slurries were extruded with a capillary nozzle of 840 μm producing layers of parallel struts with 0.8 mm spacing; the layers followed a 0º - 90º stacking scheme. The resulting components possessed a higher porosity compared to the beads (67.2 ± 0.2% for 3D_GP_C242 and 63.21 ± 0.02% for 3D_GP_H), yet higher mechanical strength thanks to their non-stochastic pore architecture (a maximum of 5.4 ± 0.6 MPa for 3D_GP_H compared to a maximum 2.1 ± 0.5 MPa for B_GP_C242).

In general, printed lattices showed higher SSA compared to beads, possibly due to the formation of a denser skin on the beads' surface; SSA was much higher for samples containing activated carbon (185.6 $m^2 g^{-1}$ for 3D_GP_C242 compared to 25.4 $m^2 g^{-1}$ for 3D_GP_H).

The maximum experimental adsorption capacities of adsorbents for Orange II were found at optimal pH 2 for the synthesized adsorbents, and were 48.82, 47.88, 35.73 and 66.65, 25.12, 41.03 mg g^{-1} for powder, bead and lattice form of GP_H and GP_C242, respectively. The pH and adsorption isotherms showed the predominantly electrostatic adsorbate-adsorbent interactions, favorability of the adsorption process which is followed by multilayer adsorption of anionic dye on the materials. The kinetic data of the removal of Orange II by the materials were preferably fitted by the pseudo-second-order model, suggesting the abundance of adsorption active sites and the reaction between negatively charged Orange II molecules and protonated surface of the adsorbents as the rate-controlling step.

Even though the performance of geopolymer composite beads and lattices still needs to be improved, they would provide for effective alternatives for water treatment, thanks to their ease of handling and separation. Their porosity and SSA increase after usage and their mechanical strength remains adequate for the application. The DIW process offers the biggest opportunities thanks to a high permeability and the possibility to tune these and other properties with an

5. References

[1] X. Xu, B. Gao, B. Jin, Q. Yue, Removal of anionic pollutants from liquids by biomass materials: A review, Journal of Molecular Liquids. 215 (2016) 565–595. https://doi.org/10.1016/j.molliq.2015.12.101.

[2] United Nations World Water Assessment Programme (WWAP), The United Nations World Water Development Report 2017 Wastewater: The Untapped Resource, Journal of Physics A: Mathematical and Theoretical. 44 (2011) 085201.

[3] K.S. Bharathi, S.T. Ramesh, Removal of dyes using agricultural waste as low-cost adsorbents: a review, Applied Water Science. 3 (2013) 773–790. https://doi.org/10.1007/s13201-013-0117-y.

[4] C.I. Pearce, J.R. Lloyd, J.T. Guthrie, The removal of colour from textile wastewater using whole bacterial cells: A review, Dyes and Pigments. 58 (2003) 179–196. https://doi.org/10.1016/S0143-7208(03)00064-0.

[5] S. Samsami, M. Mohamadi, M.H. Sarrafzadeh, E.R. Rene, M. Firoozbahr, Recent advances in the treatment of dye-containing wastewater from textile industries: Overview and perspectives, Process Safety and Environmental Protection. 143 (2020) 138–163. https://doi.org/10.1016/J.PSEP.2020.05.034.

[6] T.S. Anantha Singh, S.T. Ramesh, New trends in electrocoagulation for the removal of dyes from wastewater: A review, Environmental Engineering Science. 30 (2013) 333–349. https://doi.org/10.1089/ees.2012.0417.

[7] P.M. Mwanamoki, N. Devarajan, B. Niane, P. Ngelinkoto, F. Thevenon, J.W. Nlandu, P.T. Mpiana, K. Prabakar, J.I. Mubedi, C.G. Kabele, W. Wildi, J. Poté, Trace metal distributions in the sediments from river-reservoir systems: case of the Congo River and Lake Ma Vallée, Kinshasa (Democratic Republic of Congo), Environmental Science and Pollution Research 2014 22:1. 22 (2014) 586–597. https://doi.org/10.1007/S11356-014-3381-Y.

[8] F.A. Armah, R. Quansah, I. Luginaah, A Systematic Review of Heavy Metals of Anthropogenic Origin in Environmental Media and Biota in the Context of Gold Mining in Ghana, International Scholarly Research Notices. 2014 (2014) 1–37. https://doi.org/10.1155/2014/252148.

[9] R. El Khatib, R.S. Lartiges, A. El Samrani, P. Faure, J. Houhou, J. Ghanbaja, Speciation

Uncontrolled Urban Expansion Increases the Contamination of the Titicaca Lake Basin (El Alto, La Paz, Bolivia), 228 1–17.

[12] V. Sridhar, M.M. Billah, J.W. Hildreth, Coupled Surface and Groundwater Hydrological Modeling in a Changing Climate, Groundwater. 56 (2018) 618–635. https://doi.org/10.1111/GWAT.12610.

[13] N.K. Lazaridis, G.Z. Kyzas, A.A. Vassiliou, D.N. Bikiaris, Chitosan derivatives as biosorbents for basic dyes, Langmuir. 23 (2007) 7634–7643. https://doi.org/10.1021/la700423j.

[14] H. Singh, G. Chauhan, A.K. Jain, S.K. Sharma, Adsorptive potential of agricultural wastes for removal of dyes from aqueous solutions, Journal of Environmental Chemical Engineering. 5 (2017) 122–135. https://doi.org/10.1016/j.jece.2016.11.030.

[15] D. Jiang, M. Chen, H. Wang, G. Zeng, D. Huang, M. Cheng, Y. Liu, W. Xue, Z.W. Wang, The application of different typological and structural MOFs-based materials for the dyes adsorption, Coordination Chemistry Reviews. 380 (2019) 471–483. https://doi.org/10.1016/j.ccr.2018.11.002.

[16] Q. Yang, Y. Wang, J. Wang, F. Liu, N. Hu, H. Pei, W. Yang, Z. Li, Y. Suo, J. Wang, High effective adsorption/removal of illegal food dyes from contaminated aqueous solution by Zr-MOFs (UiO-67), Food Chemistry. 254 (2018) 241–248. https://doi.org/10.1016/j.foodchem.2018.02.011.

[17] A.A. Siyal, M.R. Shamsuddin, M.I. Khan, N.E. Rabat, M. Zulfiqar, Z. Man, J. Siame, K.A. Azizli, A review on geopolymers as emerging materials for the adsorption of heavy metals and dyes, Journal of Environmental Management. 224 (2018) 327–339. https://doi.org/10.1016/j.jenvman.2018.07.046.

[18] L. Li, S. Wang, Z. Zhu, Geopolymeric adsorbents from fly ash for dye removal from aqueous solution, Journal of Colloid and Interface Science. 300 (2006) 52–59. https://doi.org/10.1016/j.jcis.2006.03.062.

[19] J. Davidovits, Geopolymer chemistry and applications, 5th ed., Institut Geopolymere, 2020.

[20] S. Onutai, T. Kobayashi, P. Thavorniti, S. Jiemsirilers, Removal of Pb2+, Cu2+, Ni2+, Cd2+ from Wastewater using Fly Ash Based Geopolymer as an Adsorbent, Key

[23] C. Bai, G. Franchin, H. Elsayed, A. Zaggia, L. Conte, H. Li, P. Colombo, High-porosity geopolymer foams with tailored porosity for thermal insulation and wastewater treatment, Journal of Materials Research. 32 (2017) 3251–3259. https://doi.org/10.1557/jmr.2017.127.

[24] G. Franchin, J. Pesonen, T. Luukkonen, C. Bai, P. Scanferla, R. Botti, S. Carturan, M. Innocentini, P. Colombo, Removal of ammonium from wastewater with geopolymer sorbents fabricated via additive manufacturing, Materials and Design. 195 (2020) 109006. https://doi.org/10.1016/j.matdes.2020.109006.

[25] E. Landi, V. Medri, E. Papa, J. Dedecek, P. Klein, P. Benito, A. Vaccari, Alkali-bonded ceramics with hierarchical tailored porosity, Applied Clay Science. 73 (2013) 56–64. https://doi.org/10.1016/j.clay.2012.09.027.

[26] E. Papa, M. Mor, A. Natali Murri, E. Landi, V. Medri, Ice-templated geopolymer beads for dye removal, Journal of Colloid and Interface Science. 572 (2020) 364–373. https://doi.org/10.1016/J.JCIS.2020.03.104.

[27] Y. Ge, X. Cui, Y. Kong, Z. Li, Y. He, Q. Zhou, Porous geopolymeric spheres for removal of Cu(II) from aqueous solution: Synthesis and evaluation, Journal of Hazardous Materials. 283 (2015) 244–251. https://doi.org/10.1016/j.jhazmat.2014.09.038.

[28] S. Tome, D.T. Hermann, V.O. Shikuku, S. Otieno, Synthesis, characterization and application of acid and alkaline activated volcanic ash-based geopolymers for adsorptive remotion of cationic and anionic dyes from water, Ceramics International. 47 (2021) 20965–20973. https://doi.org/10.1016/J.CERAMINT.2021.04.097.

[29] A.A. Siyal, M.R. Shamsuddin, S.H. Khahro, A. Low, M. Ayoub, Optimization of synthesis of geopolymer adsorbent for the effective removal of anionic surfactant from aqueous solution, Journal of Environmental Chemical Engineering. 9 (2021) 104949. https://doi.org/10.1016/J.JECE.2020.104949.

[30] A.A. Siyal, M.R. Shamsuddin, N.E. Rabat, M. Zulfiqar, Z. Man, A. Low, Fly ash based geopolymer for the adsorption of anionic surfactant from aqueous solution, Journal of Cleaner Production. 229 (2019) 232–243. https://doi.org/10.1016/J.JCLEPRO.2019.04.384.

[31] T. Luukkonen, J. Yliniemi, H. Sreenivasan, K. Ohenoja, M. Finnilä, G. Franchin, P. Colombo, Ag- or Cu-modified geopolymer filters for water treatment manufactured by

[34] C. Bai, P. Colombo, Processing, properties and applications of highly porous geopolymers: A review, Ceramics International. 44 (2018) 16103–16118. https://doi.org/10.1016/j.ceramint.2018.05.219.

[35] G. Franchin, P. Scanferla, L. Zeffiro, H. Elsayed, A. Baliello, G. Giacomello, M. Pasetto, P. Colombo, Direct ink writing of geopolymeric inks, Journal of the European Ceramic Society. 37 (2017). https://doi.org/10.1016/j.jeurceramsoc.2017.01.030.

[36] R.F. Botti, M.D.M. Innocentini, T.A. Faleiros, M.F. Mello, D.L. Flumignan, L.K. Santos, G. Franchin, P. Colombo, Additively manufactured geopolymer structured heterogeneous catalysts for biodiesel production, Applied Materials Today. 23 (2021) 101022. https://doi.org/10.1016/j.apmt.2021.101022.

[37] L.K. dos Santos, R.F. Botti, M.D. de M. Innocentini, R.F.C. Marques, P. Colombo, A.V. de Paula, D.L. Flumignan, 3D printed geopolymer: An efficient support for immobilization of Candida rugosa lipase, Chemical Engineering Journal. 414 (2021) 128843. https://doi.org/10.1016/J.CEJ.2021.128843.

[38] P. Scanferla, A. Conte, A. Sin, G. Franchin, P. Colombo, The effect of fillers on the fresh and hardened properties of 3D printed geopolymer lattices, Open Ceramics. 6 (2021) 100134. https://doi.org/10.1016/J.OCERAM.2021.100134.

[39] T. Luukkonen, A. Heponiemi, H. Runtti, J. Pesonen, J. Yliniemi, U. Lassi, Application of alkali-activated materials for water and wastewater treatment: a review, Reviews in Environmental Science and Biotechnology. 18 (2019) 271–297. https://doi.org/10.1007/s11157-019-09494-0.

[40] B. Coppola, J.-M. Tulliani, P. Antonaci, P. Palmero, Role of Natural Stone Wastes and Minerals in the Alkali Activation Process: A Review, Materials 2020, Vol. 13, Page 2284. 13 (2020) 2284. https://doi.org/10.3390/MA13102284.

[41] S. Akazdam, M. Chafi, W. Yassine, B. Gourich, Removal of Acid Orange 7 dye from aqueous solution using the exchange resin Amberlite FPA-98 as an efficient adsorbent: Kinetics, isotherms, and thermodynamics study, Journal of Materials and Environmental Science. 8 (2017) 2993–3012.

[42] R. Heydari, M. Hosseini, A. Amraei, A. Mohammadzadeh, Preparation of a novel pH optical sensor using orange (II) based on agarose membrane as support, Materials Science and Engineering: C. 61 (2016) 333–337.

[45] F. Güzel, H. Sayğili, G.A. Sayğili, F. Koyuncu, Elimination of anionic dye by using nanoporous carbon prepared from an industrial biowaste, Journal of Molecular Liquids. 194 (2014) 130–140. https://doi.org/10.1016/J.MOLLIQ.2014.01.018.

[46] R. Saadi, Z. Saadi, R. Fazaeli, N.E. Fard, Monolayer and multilayer adsorption isotherm models for sorption from aqueous media, Korean Journal of Chemical Engineering 2015 32:5. 32 (2015) 787–799. https://doi.org/10.1007/S11814-015-0053-7.

[47] C.R. Minitha, M. Lalitha, Y.L. Jeyachandran, L. Senthilkumar, R.T. Rajendra Kumar, Adsorption behaviour of reduced graphene oxide towards cationic and anionic dyes: Co-action of electrostatic and $\pi - \pi$ interactions, Materials Chemistry and Physics. 194 (2017) 243–252. https://doi.org/10.1016/J.MATCHEMPHYS.2017.03.048.

[48] J. Wang, X. Guo, Adsorption kinetic models: Physical meanings, applications, and solving methods, Journal of Hazardous Materials. 390 (2020) 122156. https://doi.org/10.1016/J.JHAZMAT.2020.122156.

[49] R. Rajbhandari, L.K. Shrestha, R.R. Pradhananga, Preparation of Activated Carbon from Lapsi Seed Stone and its Application for the Removal of Arsenic from Water, Journal of the Institute of Engineering. 8 (2011) 211–218. https://doi.org/10.3126/JIE.V8I1-2.5113.

[50] W.W. Focke, D. Molefe, F.J.W. Labuschagne, S. Ramjee, The influence of stearic acid coating on the properties of magnesium hydroxide, hydromagnesite, and hydrotalcite powders, Journal of Materials Science 2009 44:22. 44 (2009) 6100–6109. https://doi.org/10.1007/S10853-009-3844-6.

[51] F.J.W.J. Labuschagné, A. Wiid, H.P. Venter, B.R. Gevers, A. Leuteritz, Green synthesis of hydrotalcite from untreated magnesium oxide and aluminum hydroxide, Http://Mc.Manuscriptcentral.Com/Tgcl. 11 (2018) 18–28. https://doi.org/10.1080/17518253.2018.1426791.

[52] E. M. Cepollaro, R. Botti, G. Franchin, L. Lisi, P. Colombo, S. Cimino, Cu/ZSM5-Geopolymer 3D-Printed Monoliths for the NH3-SCR of NOx, Catalysts 2021, 11, 1212. https://doi.org/10.3390/catal11101212

[53] E. Papa, E. Landi, A. Natali Murri, F. Miccio, A. Vaccari, V. Medri, CO_2 adsorption at intermediate and low temperature by geopolymer-hydrotalcite composites, Open Ceramics, 2021, 5, 100048, https://doi.org/10.1016/j.oceram.2020.100048.